ELSEVIER

Journal of Power Sources 87 (2000) 118–124

JOURNAL OF POWER SOURCES

www.elsevier.com/locate/jpowsour

# Effects of Zr addition on discharge properties of mechanically alloyed $Mg_2Ni$ hydrogen-storage alloy electrode

Nam Hoon Goo *, Woon Tae Jeong, Kyung Sub Lee

*Division of Materials Science and Engineering, Hanyang University, Seoul 133-791, South Korea*

Received 17 August 1999; accepted 2 October 1999

**Abstract**

$(Mg_{1-x}Zr_x)_2Ni$ ($x = 0.0$, 0.1, 0.2, 0.3 and 0.4) hydrogen-storage alloy electrodes are synthesized by means of a mechanical alloying process using a planetary ball mill. After milling for 160 h, $(Mg_{1-x}Zr_x)_2Ni$ alloy with $x = 0.0$ remained the nanocrystalline phase. By contrast, Zr addition to this alloy enhances the structural disorder and amorphization. The discharge capacity of a $(Mg_{1-x}Zr_x)_2Ni$ electrode increases with Zr content and reaches the highest capacity of 530 mAh $g^{-1}$ at $x = 0.3$, then decreases to 230 mAh $g^{-1}$ at $x = 0.4$, i.e., lower than that of pure $Mg_2Ni$. Cyclic stability and rate capability vary with Zr addition. 

*Keywords:* $Mg_2Ni$ phase; Nanocrystalline; Zr addition; Amorphous phase; Discharge capacity; Hydrogen-storage

## 1. Introduction

$Mg_2Ni$ type metal hydride electrodes have been studied extensively in the recent years because of their large hydrogen capacity, low cost, light weight and non-toxicity. The polycrystalline $Mg_2Ni$ phase however, forms a stable hydride, $Mg_2NiH_4$, which is unable to desorb hydrogen at room temperature and shows a very low electrochemical discharge capacity. In addition, the conventional arc-melting process to synthesize the $Mg_2Ni$ phase presents some difficulties due to the large difference in the melting points of the two elements, and segregation problems. Some researchers have tried to overcome these drawbacks by employing a mechanical alloying process [1–3]. In our previous work [4], the nanocrystalline $Mg_2Ni$ phase was successfully synthesized by mechanical alloying. The grain size of the mechanically alloyed $Mg_2Ni$ phase was less than 50 nm, and the discharge capacity reached 200 mAh $g^{-1}$ at room temperature. Although application of a mechanical alloying process for producing $Mg_2Ni$ alloy looks promising, there still exist the problems of low discharge capacity, the poor cycle life, and poor high-rate discharge capability.

The theoretical discharge capacity of the $Mg_2Ni$ phase, assuming the formation of the $Mg_2NiH_4$, is 999 mAh $g^{-1}$, but the experimentally measured discharge capacity of the mechanically alloyed $Mg_2Ni$ phase is only 200 mAh $g^{-1}$, which is far less than that of other hydrogen-storage alloys. Therefore, methods for increasing the discharge capacity are required.

The cycle life of the mechanically alloyed $Mg_2Ni$ phase is so poor that only about 20% of the maximum capacity remains after 10 cycles. It has been suggested that this is due to the fast oxidation of Mg and the formation of a thick passive layer [4]. Together with the formation of a passive oxide layer, the slow hydriding kinetics of the $Mg_2Ni$ phase severely inhibit the rate capability. Consequently, the discharge capacity is usually measured at a very low discharge density (e.g., 10 mA $g^{-1}$). It has been reported [4,5] that modification of alloy surface is effective in preventing oxidation of Mg and also enhances the hydriding reaction. The addition of various ternary elements into $Mg_2Ni$ has been also investigated [6–8] to improve the hydriding kinetics and the discharge capacity of the hydride.

In this work, ternary Mg–Ni–Zr alloys with various compositions have been prepared by a mechanical alloying process. Structural characterization has been carried out, and the electrochemical properties of the alloy powders have been investigated.

* Corresponding author. Tel.: +82-2-2281-4914; fax: +82-2-2281-4914; e-mail: laves@hymail.hanyang.ac.kr

0378-7753/00/$ - see front matter 
PII: S0378-7753(99)00432-2

## 2. Experimental

Elemental Mg and Ni powders were mixed with Zr powder in various compositions. The composition of the powder mixture was described as $(Mg_{1-x}Zr_x)_2Ni$. Here, $(Mg_{1-x}Zr_x)_2Ni$ refers only to the composition of the powder mixture, and does not consider that Zr has substituted a Mg site or a Ni site after mechanical alloying. The compositional ratios were $x = 0.0$, 0.1, 0.2, 0.3, and 0.4. The mixed powders were charged into Cr–Ni steel vials with Cr–Ni steel balls of 2/16 in. size. The ball to powder ratio was 15:1. The mechanical alloying was performed under an argon atmosphere with a planetary ball mill (Fritsch, Pulverisette P-5). The milling speed was 100 rpm and the duration time was 160 h, while the milling time in our previous work was 120 h [1]. The milling time was increased because the Zr addition was greater.

Structural and morphological properties of the alloy powders were characterized by means of X-ray diffraction (XRD, Cu Kα, Rigaku D-MAX 3000), thermal analysis (differential scanning calorimetry, DSC), and transmission electron microscopy (TEM) observation. Thermal analysis was performed under purified argon at a heating rate of 5°C $min^{-1}$ up to 600°C, with sample weight of 5.195 mg. To prepare the TEM specimens, the alloy powders were kneaded with G1 epoxy and hardener, mechanically polished to thin films of thickness of 50 μm, and then ion milled.

The composition profile of the surface of each alloy powder was investigated by atomic emission spectroscopy (AES, PHI-680, Auger Nanoprobe). Accelerated Ar + ions at 2.0 keV were sputtered on the alloy surface at a rate of 44 Å $min^{-1}$. A $SiO_2$/Si raster and the C1s peak were used to estimate the sputtering rate and to calibrate peak positions, respectively.

Working electrodes were prepared by cold pressing the alloy powders into pellets of 10 mm in diameter, under a pressure of 5.0 ton $cm^{-2}$. Electrochemical cycle tests were conducted in a half-cell which comprised the working electrode, a platinum counter electrode and a mercury/mercurous oxide (Hg/HgO) reference electrode in 6M KOH electrolyte. All potentials are reported with respect to the reference electrode. Tests were performed with an automatic galvanostatic charge–discharge unit (Maccor se-

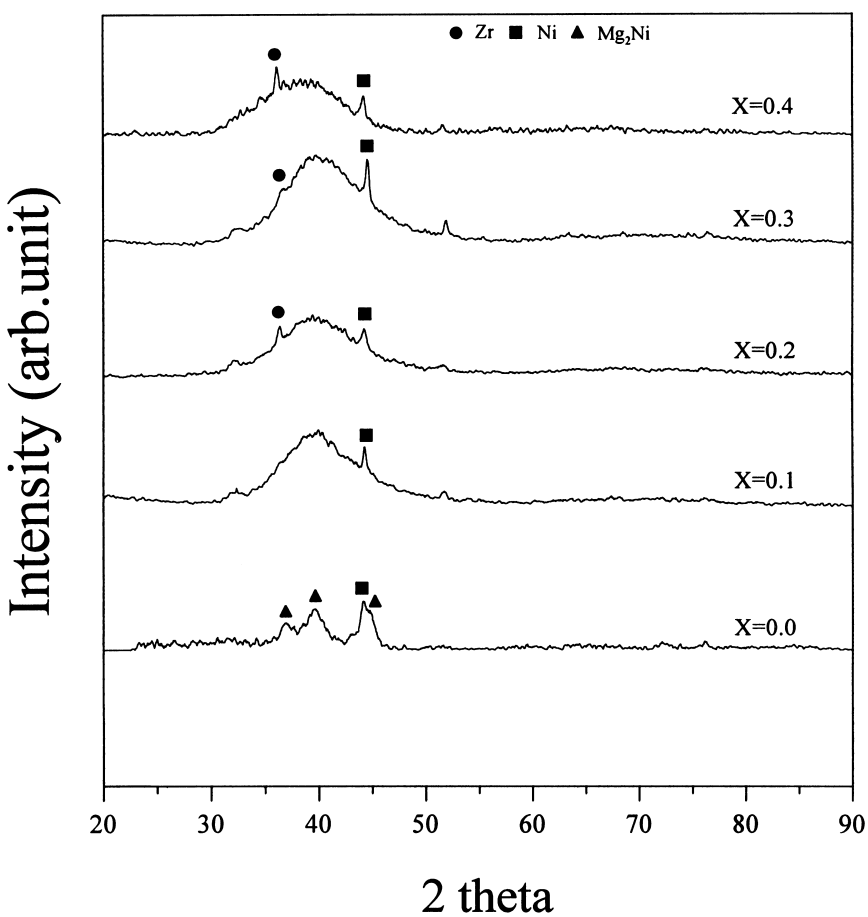


Fig. 1. XRD patterns for ball-milled $(Mg_{1-x}Zr_x)_2Ni$ alloy.

Table 1
Phases of ball-milled $(Mg_{1-x}Zr_x)_2Ni$ alloys, as determined by XRD analysis

| Alloy composition ($x$) | Phases | Relative amounts |
|---|---|---|
| 0.0 | Crystalline $Mg_2Ni$ (HCP) + Ni | $Mg_2Ni$ > Ni |
| 0.1 | Amorphous + Ni | Amorphous > Ni |
| 0.2 | Amorphous + Zr + Ni | Amorphous > Ni > Zr |
| 0.3 | Amorphous + Zr + Ni | Amorphous > Ni > Zr |
| 0.4 | Amorphous + Zr + Ni | Amorphous > Zr > Ni |

ries 4000). The charge and discharge cut-off voltage were $-0.96$ and $-0.6$ V to prevent hydrogen evolution and oxidation of the copper connectors, respectively. The charge current density was 10 mA $g^{-1}$, and the discharge current density was varied to investigate the rate capability of the $(Mg_{1-x}Zr_x)_2Ni$ electrode.

## 3. Results and discussion

### 3.1. Structure

The XRD patterns of the mechanically alloyed $(Mg_{1-x}Zr_x)_2Ni$ alloys are shown in Fig. 1, and the phases formed are listed in Table 1. The ball-milled $(Mg_{1-x}Zr_x)_2Ni$ alloy with $x = 0.0$ is composed of the nanocrystalline $Mg_2Ni$ phase and elemental Ni. The broadened $Mg_2Ni$ peaks indicate refinement of the average grain size and stored stress in the grains. The electron diffraction pattern shown in Fig. 2(c) confirms the formation of the $Mg_2Ni$ phase. The average grain size in the dark field image of Fig. 2(b) is less than 10 nm. With increasing Zr addition, the $(Mg_{1-x}Zr_x)_2Ni$ phase loses its crystalline properties. Maximum broadening of the $Mg_2Ni$ peaks was observed for $x = 0.1$ and suggests amorphization of the crystalline state. When the $x$ value is 0.2, 0.3 or 0.4, elemental Zr which has not reacted is detected. The ele-

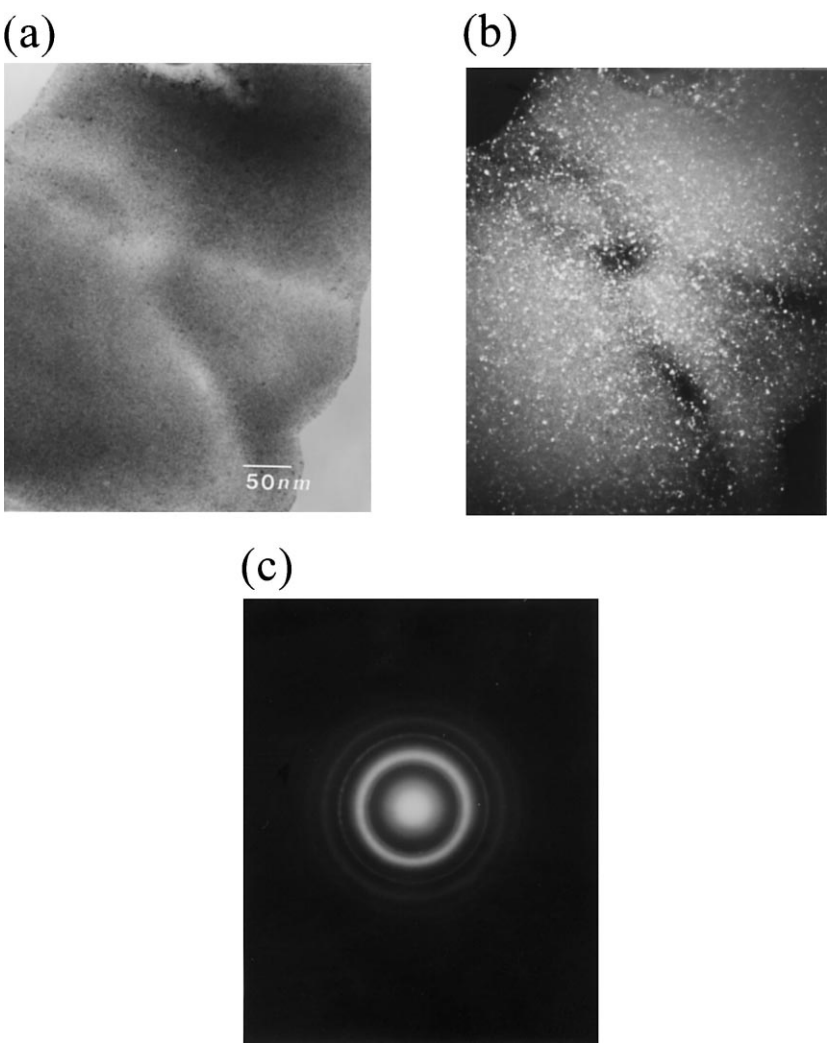


Fig. 2. TEM micrographs of $(Mg_{1-x}Zr_x)_2Ni$ alloy with $x = 0.0$, milled for 160 h.

mental Zr peak is maximum at a composition of $x = 0.4$. The AES depth profile shown in Fig. 3 indicates that the excess Zr content is more than the Mg content at the surface of the powder. This Zr-rich layer is considered to protect the oxidation of Mg, but lowers the maximum discharge capacity.

TEM micrographs of powders with composition of $x = 0.3$ are given in Fig. 4. The broad hollow ring in the SAD pattern indicates an amorphous phase. In order to examine the crystallization of the amorphous phase, DSC analysis was conducted. The resulting profile (Fig. 5) revealed that there are two major exothermic peaks at 310 and 360°C, before melting of the alloy powder. As reported by Yang et al. [9] these exothermic peaks are caused by the formation of $Mg_2Ni$ and $MgNi_2$ phases, respectively.

The reason for formation of an amorphous phase in Zr-bearing Mg–Ni alloys during mechanical alloying may be explained by the following two features.

(i) In our experiment, it was intended that Zr was substituted for Mg; the Mg content of the powder mixture decreases as Zr is added. Consequently, this gives rise to a compositional change in the Mg–Ni system from a composition of $Mg_2Ni$ (Mg–33 at.% Ni) to a composition with additional Ni. Orimo et al. [10] examined the effect of Ni content on the amorphization of the ball-milled Mg–Ni alloys. On ball milling, a $Mg_2Ni$ composition (Mg–33 at.% Ni), no amorphous phase was found to form. The amorphous phase was partially formed by ball milling a Mg–$x$ at.% Ni mixture with additional Ni ($x = 38$, 43), and a homogenous amorphous phase was produced with a composition of Mg–50 at.% Ni.

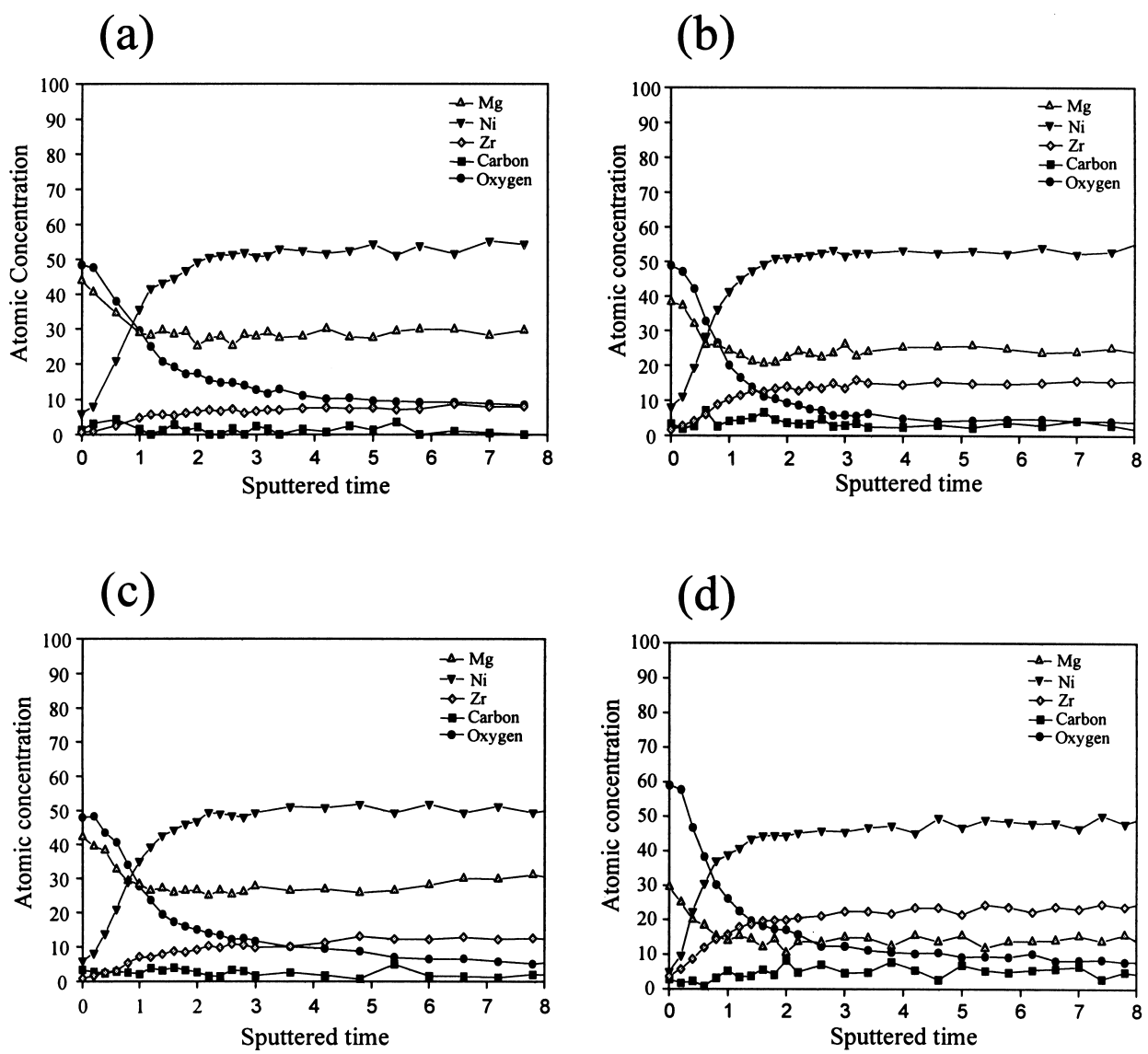


Fig. 3. AES depth profiles of $(Mg_{1-x}Zr_x)_2Ni$ alloy powder: (a) $x = 0.1$; (b) $x = 0.2$; (c) $x = 0.3$; and (d) $x = 0.4$.

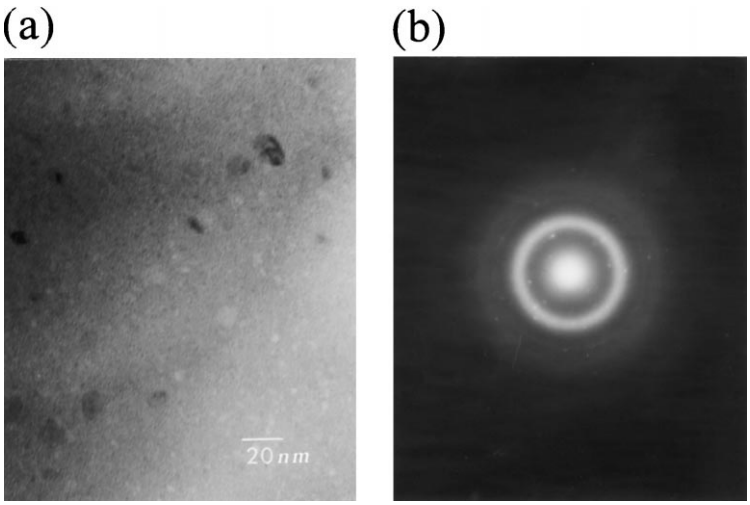


Fig. 4. TEM micrographs of $(Mg_{1-x}Zr_x)_2Ni$ alloy with $x = 0.3$, milled for 160 h.

In general, an amorphous structure can be produced by solid-state reactions in a composition range with a large negative heat of mixing [11]. Orimo et al. [10] also advocated that the heat of mixing for the equivalent composition (Mg:Ni = 1:1) was similar to that for the stable compound, and the equivalent composition in Mg–Ni system easily transformed into the amorphous phase. In our experiments, the compositional deviation from the composition of the $Mg_2Ni$ phase (Mg–33 at.% Ni), which was caused by Zr addition, enhanced the amorphization of the Mg–Ni alloy system.

(ii) The atomic radius of Zr is larger than that of Mg or Ni. Therefore, Zr addition to $Mg_2Ni$ type alloys may lead to severe volume expansion of the $Mg_2Ni$ lattice. Chakk et al. [12] advanced a model for amorphization by mechanical alloying. It was claimed that amorphization during mechanical alloying occurs as a result of penetration of impurity atoms into the host lattice and destruction of the long-range order. During the mechanical alloying of $(Mg_{1-x}Zr_x)_2Ni$ alloy, the Zr atom penetrates into the host $Mg_2Ni$ lattice, which may occupy either a substitutional or interstitial site in the $Mg_2Ni$ lattice. The Zr-bearing $Mg_2Ni$ phase may have a strained lattice structure with its volume is expanded. During ball milling of $(Mg_{1-x}Zr_x)_2Ni$ alloys, the lattice strain caused by Zr addition is coupled with the mechanical strain caused by comminution. The mechanical strain at room temperature can effectively destroy ordering of the host lattice with the help of the impurity Zr.

In the XRD patterns of Fig. 1, the amorphous phase begins to form at $x = 0.1$. With increasing Zr addition, the amorphization is increased. For $x = 0.4$, however, the excess Zr is too much to react with Mg or Ni. Amorphization at $x = 0.3$ is more effective than that of the other compositions.

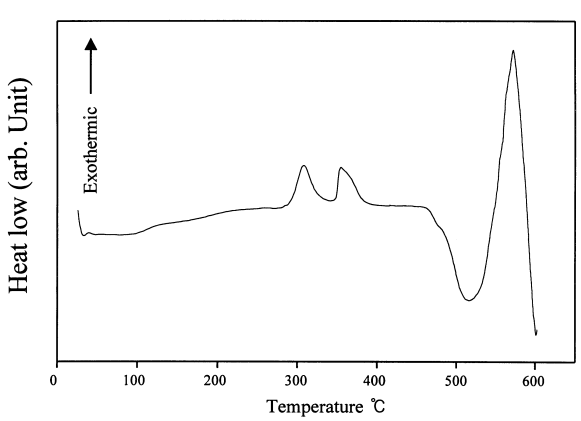


Fig. 5. DSC profile of $(Mg_{1-x}Zr_x)_2Ni$ alloy with $x = 0.1$, milled for 160 h.

### 3.2. Discharge capacity

Electrochemical cycle data for $(Mg_{1-x}Zr_x)_2Ni$ electrodes with various Zr contents within 20 cycles are shown in Fig. 6. The discharge current density was 10 mA $g^{-1}$. The discharge capacities of electrodes with compositions $x = 0.1$ and 0.3 are greatly increased. For $x = 0.0$, the $Mg_2Ni$ phase prepared by milling for 160 h exhibited a larger discharge capacity than the $Mg_2Ni$ phase subjected to 120 h of milling. The grain size of the former $Mg_2Ni$ phase was less than 10 nm, which is more refined than that of material milled for 120 h (20–50 nm) [1]. The refined grain size made the $Mg_2Ni$ phase more active towards absorption/desorption of hydrogen, which resulted in improved discharge capacity.

The $(Mg_{1-x}Zr_x)_2Ni$ electrode with $x = 0.4$ displayed the poorest discharge capacity, for which the excess Zr in the Ni-rich layer at the powder surface was responsible (see Fig. 3b). Although the Ni-rich layer has a large catalytic activity for hydrogen absorption, Zr reduces the catalytic activity, impedes hydrogen diffusion, and lowers the reversible discharge capacity of the electrode.

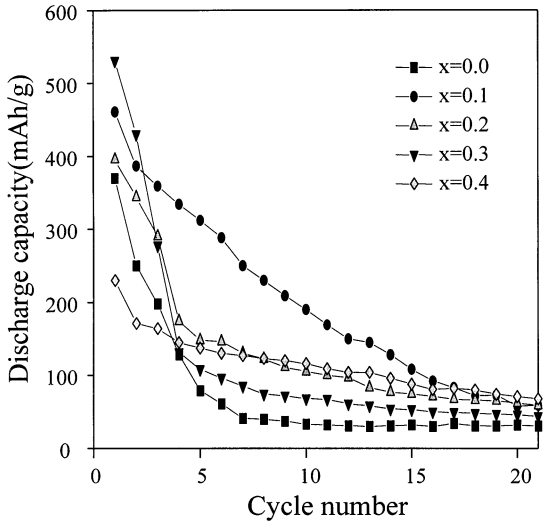


Fig. 6. Discharge capacities of $(Mg_{1-x}Zr_x)_2Ni$ alloy electrodes at 10 mA $g^{-1}$.

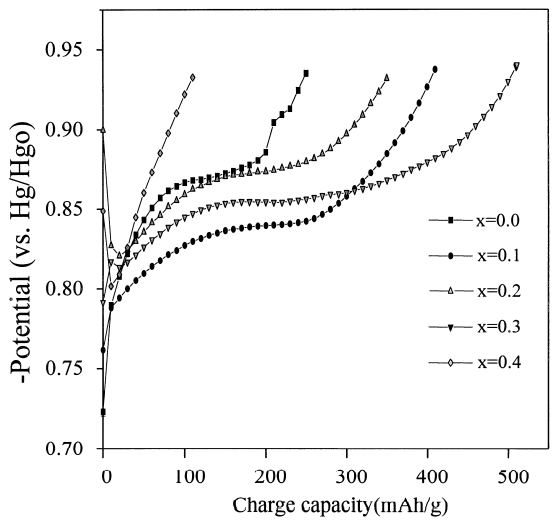


Fig. 7. Galvanostatic charge curves of $(Mg_{1-x}Zr_x)_2Ni$ alloy electrodes at 10 mA $g^{-1}$.

The increased discharge capacity of $(Mg_{1-x}Zr_x)_2Ni$ alloys ($x = 0.1, 0.2, 0.3$) may be due to the presence of an amorphous matrix. There are some conflicting reports on the hydriding/de-hydriding properties of the amorphous phase. Ryan et al. [13] reported that the discharge capacity of $Ni_{64}Zr_{36}$ amorphous alloys was 200 mAh $g^{-1}$, i.e., similar to that of conventional Ni/Cd batteries. This was due to the large reversible hydrogen solubility of the amorphous phase. Liu et al. [14], and Lee and Ha [15] reported the electrode capacity of Mg–Ni and Ti–Fe amorphous phases was greatly improved, since the diffusivity and solubility of hydrogen in amorphous phases were larger than those in crystalline phases.

According to Libowitz and Maeland [16], the absorption of hydrogen may depend not on the crystal structure but on the electro-magnetic structure. Thus, in case of the Pd–Si system, the amount of absorbed hydrogen in the crystalline phase was larger than that in the amorphous phase.

The Mg–Ni–Zr amorphous system has a large solubility of hydrogen. The galvanostatic charge curves of $(Mg_{1-x}Zr_x)_2Ni$ electrodes are shown in Fig. 7. Despite the amorphous phase, there is a potential plateau region, which is in agreement with the studies of Orimo et al. [17]. The electrode with $x = 0.3$ has the longest potential plateau region, and the highest charge capacity. Electrodes with $x = 0.1$, 0.2 also exhibit larger plateau regions than that of the electrode with $x = 0.0$. The potential plateau region is due to the following reaction of metal hydride formation.

$$M + \alpha\, H_2O + \alpha\, e^- = MH_\alpha + \alpha\, OH^- \quad (1)$$

The value of $\alpha$ in the reaction refers to the hydrogen solubility of the metal hydride and the amount of the electron flow, which is represented by the capacity during the charge process. If the metal hydride has a small hydrogen solubility or inhibits hydrogen diffusion into hydrogenation sites, there is a steep potential decrease, and a small potential plateau region.

The amorphous phases formed for $x = 0.1$, 0.2 and 0.3 have a longer plateau region than the nanocrystalline phase formed for $x = 0.0$, which is associated with a large hydrogen solubility. The $(Mg_{1-x}Zr_x)_2Ni$ electrode with $x = 0.4$ has a low charge capacity and a large potential drop since the surface contains more Zr than that of other electrodes. The elemental Zr has no ability to electrochemically absorb hydrogen, rather it blocks hydrogen diffusion.

The degradation in the discharge capacity of $(Mg_{1-x}Zr_x)_2Ni$ electrodes is so severe that about 70% of the maximum capacity is lost within 20 cycles; the loss of the capacity for the electrode with $x = 0.4$ is 50% of

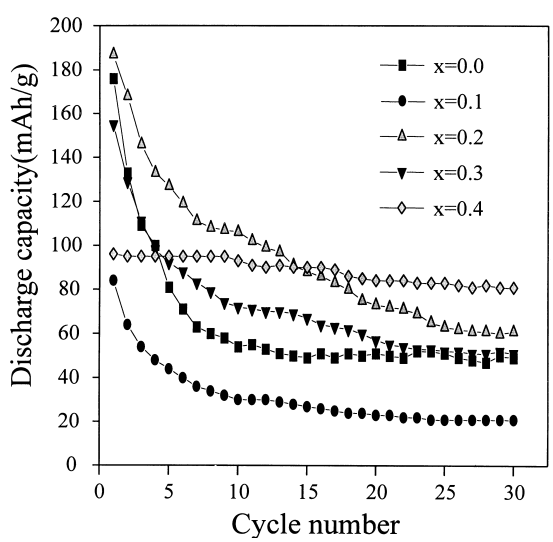


Fig. 8. Discharge capacities of $(Mg_{1-x}Zr_x)_2Ni$ alloy electrodes at 50 mA $g^{-1}$.

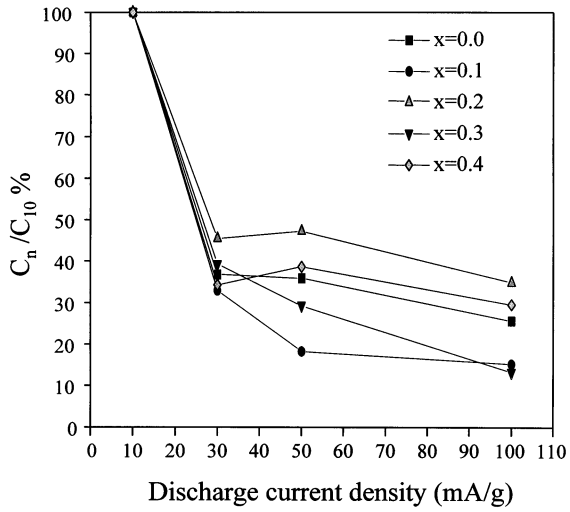


Fig. 9. Rate capability of $(Mg_{1-x}Zr_x)_2Ni$ alloy electrodes.

maximum capacity at 10 mA $g^{-1}$. At the surface of the electrode with $x = 0.4$, the amount of Zr is more than that of Mg. This surface exhibits resistance to the oxidation of Mg. The good cycle life of the electrode with $x = 0.4$ is due to the retardation of the passive $Mg(OH)_2$ formation. The $Mg_{1.2}Zr_{0.8}Ni$ electrode also shows good cycle life, even at the higher discharge rate of 50 mAh $g^{-1}$ (Fig. 8).

### *3.3. Rate capability*

Rate capability is one of the important properties for the development of a high-performance battery because it is related to the power density of the battery. The hydriding kinetics, which determines the high-rate discharge ability, is dependent upon the hydrogen diffusion and the charge-transfer reaction at the electrode surface. In these studies, the rate capability is defined as the ratio of discharge capacity at $n$ mA $g^{-1}$, $C_n$, and at 10 mA $g^{-1}$, $C_{10}$, (i.e., $C_n/C_{10}$. The rate capability of $(Mg_{1-x}Zr_x)_2Ni$, electrodes at room temperature is shown in Fig. 9. Zr additions do not greatly improve the discharge rate of these electrodes. The discharge capacity at 30 mA $g^{-1}$ decreased rapidly, and was less than 50% of the discharge capacity at 10 mA $g^{-1}$ for $(Mg_{1-x}Zr_x)_2Ni$ ($x = 0.0$, 0.1, 0.2, 0.3, 0.4) electrodes. It is known that the amorphous phase has high diffusivity and high catalytic activity [14]. The amorphous phase however, has high catalytic activity for the oxidation reaction as well as the hydrogen absorption reaction. At the higher current densities, the oxidation reaction is superior to the hydrogenation reaction.

Electrodes with compositions of $x = 0.2$ and 0.4, for which XRD analysis showed remaining Zr peaks, had a slightly improved rate capability. It is considered that the remaining Zr hinders the oxidation of Mg. The discharge capacity at 50 mA $g^{-1}$ was about 48% of that at 10 mA $g^{-1}$ for the electrode with $x = 0.4$, while for the electrode with $x = 0.2$ the discharge capacity at 50 mA $g^{-1}$ was 38% of that at 10 mA $g^{-1}$. This difference is also due to the fact that the amount of Zr at $x = 0.4$ is more than that at $x = 0.2$. The Zr-rich layer of the electrode with $x = 0.4$ may have a positive effect in retarding the formation of passive $Mg(OH)_2$, but may have a negative effect in providing an obstacle for hydrogen diffusion through the catalytic Ni-rich layer.

## 4. Conclusions

A $(Mg_{1-x}Zr_x)_2Ni$ type hydrogen-storage alloy is synthesized by mechanical alloying process. Additions of Zr enhanced appreciably the structural disorder and a ternary amorphous phase of Mg–Ni–Zr is formed. Because of the formation of this amorphous phase, the maximum discharge capacity is increased to 530 mAh $g^{-1}$. On the other hand, the degradation rate and the rate capability are not greatly improved by Zr addition.

## Acknowledgements

The authors wish to acknowledge the financial support of the Korea Research Foundation made in the program year of 1998.

## References

[1] J.H. Woo, K.S. Lee, J. Electrochem. Soc. 146 (3) (1999) 819–823.
[2] W. Liu, H. Wu, Y. Lei, Q. Wang, J. Wu, J. Alloys Compd. 252 (1997) 234–237.
[3] M. Abdellaoui, D. Cracco, A. Percheron-Guegan, J. Alloys Compd. 268 (1998) 233–240.
[4] N.H. Goo, J.H. Woo, K.S. Lee, J. Alloys Compd. 288 (1999) 286–293.
[5] J.L. Luo, N. Cui, J. Alloys Compd. 264 (1998) 299–305.
[6] N. Cui, B. Luan, H.J. Zhao, H.K. Liu, S.X. Dou, J. Alloys Compd. 233 (1996) 236–240.
[7] W. Liu, H. Wu, Y. Lei, Q. Wang, J. Wu, J. Alloys Compd. 261 (1997) 289–294.
[8] T. Kohno, M. Kanda, J. Electrochem. Soc. 144 (7) (1977) 2384–2388.
[9] Q.M. Yang, Y.Q. Lei, C.P. Chen, J. Wu, Q.D. Wang, G.L. Lu, L.S. Chen, Z. Phys. Chem. 183 (1994) 141–147.
[10] S. Orimo, K. Ikeda, H. Fujii, Y. Fujikawa, Y. Kitano, K. Yamamoto, Acta Mater. 45 (6) (1997) 2271–2278.
[11] P.H. Shingu, K.N. Ishihara, J. Alloys Compd. 194 (1993) 234–319.
[12] Y. Chakk, S. Berger, B.-Z. Weis, E. Brook-Levinson, Acta Mater. 42 (11) (1994) 3679–3685.
[13] D.H. Ryan, F. Dumais, B. Patel, J. Kycia, J.O. Strom-Olsen, J. Less-Common Met. 172–174 (1991) 1251–1296.
[14] W. Liu, Y. Lei, D. Sun, J. Wu, Q. Wang, J. Power Sources 58 (1996) 243–247.
[15] K.S. Lee, C.J. Ha, Korean J. Mater. Res. 5 (1) (1995) 112–120.
[16] G.G. Libowitz, A.J. Maeland, J. Less-Common Met. 101 (1984) 131–143.
[17] S. Orimo, K. Ikeda, H. Fujii, S. Saruki, T. Fukunaga, A. Zuttel, L. Schlapbach, Acta Mater. 46 (13) (1998) 4519–4525.